

Exploring the Impact of Affine Loop Transformations in Qubit Allocation

Martin Kong

The University of Oklahoma
Norman, OK, USA
mkong@ou.edu

Abstract

Most quantum compiler transformations and qubit allocation techniques to date are either peep-hole focused or rely on sliding windows that depend on a number of external parameters. Thus, global optimization criteria are still lacking. In this paper we explore the synergies and impact of affine loop transformations in the context of qubit allocation and mapping. With this goal in mind, we have implemented a domain specific language and source-to-source compiler for quantum circuits that can be directly described with affine relations. We conduct an extensive evaluation spanning 8 quantum circuits taken from the literature, 3 distinct coupling graphs, 4 affine transformations (including the Pluto dependence distance minimization and Feautrier’s minimum latency algorithms), and 4 qubit allocators. Our results demonstrate that affine transformations using global optimization criteria can cooperate effectively in several scenarios with quantum qubit mapping algorithms to reduce the circuit depth, size and allocation time.

Keywords: affine compilation, polyhedral model, quantum computing, qubit allocation

1 Introduction

The field of Quantum Computing (QC) has made tremendous advances in the last two decades at the hardware (e.g. ion trap and superconducting QC), algorithmic (QFT [7, 18, 19, 34], Grover’s Search [14, 33, 43], Shor’s algorithm [10, 45, 51, 60, 61]), and software levels [21, 52, 58]. Known quantum algorithms already provide us with a glimpse of their expected exceptional complexity. Thus, it is imperative for a programming language to be a vehicle for algorithmic specification rather than an obstacle in the path to progress. To address and bridge the semantic gap between algorithm specification and quantum architectures, several languages, compilers and frameworks have been proposed. Examples of these are ProjectQ [67], Scaffold and the ScaffCC compiler [40], Quipper [30], Microsoft’s Q# DSL [68] and SIMD approaches such as [36], or approaches focused on safe uncomputation such as SILQ [11].

Ultimately, the high-level programming language produces a stream of quantum assembly operations [12, 21], at which point *Qubit Allocation*, a technique akin to classic register allocation [15, 56], is applied to find a space-time mapping of

the quantum gate operations in the program to the quantum device. Qubit allocation techniques typically decompose the input program into (network) layers, and generally suffer from limitations such as approximating the global solution from local optima [37], use relative small sliding windows [48], leverage random initial mappings [37, 62], or incur in high time and space complexity due to exponentially large search spaces [35, 81].

The main goal of this work is to explore and understand potential synergistic interactions between affine loop transformations and qubit allocation techniques in order to find scenarios where the power of a global optimization criteria can effectively improve the quality of the qubit allocation. Our evaluation shows that even state-of-the-art allocators such as **sabre** [48] can improve by as much as 34% with classical polyhedral loop transformations, while other techniques less computationally demanding (i.e. **wpm** [62]) can improve by up to 60%¹.

In summary, this paper makes the following contributions: i) We conduct an extensive study to understand the interactions of affine loop transformations with qubit allocation techniques. Our evaluation encompasses 8 quantum circuits, 4 allocators, 3 topologies and 3 affine transformations in addition to the pass through code generation mode. ii) Inspired in the Omega calculator [41] and ISCC’s [76] notation, we introduce a simple domain specific language based on polyhedral abstractions to enable the description, manipulation and composition of quantum circuits. iii) We discuss how the polyhedral model can be used as an efficient intermediate representation for the optimization of affine quantum circuits. In particular, we highlight how we can use it to represent quantum networks.

The rest of this paper is organized as follows. Sec.2 recaps the necessary quantum terminology and background. In particular, we briefly recap several quantum allocators recently introduced, and which we use in our evaluation. Sec.3 revises the polyhedral background while introducing a simple domain-specific language for affine quantum circuits. Sec.4 discusses our extensive evaluation, general results, individual analyses and scalability tests. We conclude this paper with the related work (Sec.5) and the final remarks in Sec.6.

¹**sabre**’s average improvement over **jku** for large circuits is 14%, reported in [48]

2 Background in Quantum Computing

Qubits Quantum bits are the basic unit of information of quantum programs, and are the analogous of classical bits. However, unlike their classical counterpart, which can only take the values in the set $\{0,1\}$, qubit values take the form of linear combinations of two basis states ($|0\rangle$ and $|1\rangle$).

Gates and Measurement Are the elementary operations applied to qubits. Their role is to evolve the state of qubits. More generally, quantum gates can be seen as unitary matrix operations applied to vectors representing quantum states. Current quantum technologies utilize gate operations with 1 and up to 3 qubits. An example of a single qubit operation is the NOT (X) gate, which negates the state of a single qubit. An example of a two-qubit gate is the CNOT (Controlled-NOT or CX) operation, which reverses the state of the second qubit operand when the first one is 1. An example of a 3-qubit gate is the CCNOT (Controlled-Controlled-NOT), which utilizes two control and one target qubits. In terms of classical computing the control-qubits are *read-only* while the target qubit is effectively *updated*. Quantum gates are akin to assembly code in classical computing.

Coupling Graphs A quantum processor can be conceptually conceived as a graph/network where the vertices are the qubits, and the edges the communication links between them. Computational steps (gates) performed in the network are synchronized in time. Qubits serve as inputs and outputs to each quantum operation. A current limitation of quantum computing technology, is that multi-qubit gates can only be applied to qubits directly connected by a link [44, 80].

Quantum Circuits Quantum programs can be graphically represented in the form of circuits [71]. We show an example of a simple circuit obtained from the Revlib online repository [59] in Fig.1. The x-axis signifies time, while the y-axis are the qubits available in the quantum processor. It uses 6 qubits, 5 NOT gates (left-most), and 5 CNOT gates. Each NOT gate is synchronized with the control qubit of a CNOT gate. Operations on the same qubit lane, from left-to-right execute one-after another, and embody classic data-flow input/output dependences.

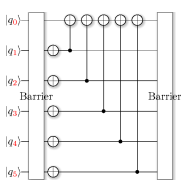


Figure
parity_247
circuit [59]

1. The actual semantics of the specific gate determine if the state of a qubit q_i is read, written, or both. The *depth* of a quantum circuit is the maximum number of gates scheduled on any single qubit lane, whereas the total number of gates is the *circuit size*. The quantum circuit ultimately defines the unitary evolution of the input (initial) state into the final/output state.

Qubit Allocation Is the space-time mapping (assignment) of quantum operations to qubits in the coupling graph, and is very similar in spirit to the classical register allocation

problem. Recently several qubit allocators have been proposed. We briefly summarize a few of the most relevant techniques. The **ibm-mapper** [37] (available in Qiskit) divides the input into a sequence of layers using disjoint sets of qubits; qubits within layers are mapped by minimizing the sum of squared distances among vertices, and potentially inserting SWAP operations. In addition, each distance term is scaled by a factor $1 + r$, where r is a random number between 0 and 1. The algorithm defaults to one gate per layer if a valid mapping is not found. **wpm** [62] is a heuristic that finds first an initial allocation maximizing the number of control dependences, followed by a second pass which completes any remaining ordering constraint, potentially inserting SWAP operations. Siraichi et al. [62] also proposed an exact solution to the qubit allocation problem as a dynamic program with state memoization, and showing that it leads to a $O(|Q|^2 \cdot |Q| \cdot |D|)$, where Q is the set of (physical) qubits, and D the list of dependences. The heuristic proposed (**wpm**) was shown to achieve $O(|Q| \cdot \lg(|Q|) + |E| + |D| + |D| \cdot (|Q| + |E|))$. **jku** [81] uses the circuit size as the main optimizing metric, decomposing the input network into layers, and attempting to minimize the number of gates within each layer. To avoid falling into local optima, **jku** uses an A* search algorithm [35], a family of graph traversal algorithms known to incur in $O(b^d)$ space complexity, where b is the branching factor in a tree and d its depth. The heuristic used to drive the search attempts to convert the mapping of each layer into the subsequent one by inserting SWAP operations. **sabre** [48] is an efficient algorithm with $O(N^{2.5}g)$ time complexity that attempts to minimize both the circuit depth and size, usually exploring a trade-off between them. As previous techniques, it divides the input program into layers, but performs two additional passes (a back-traversal and a second forward traversal) to improve the initial (random) mapping.

(De)Coherence One of the main challenges facing QC is the decoherence problem, where the state of a qubit decays over time. Each quantum gate has a specific decoherence time, which for state-of-the-art quantum machines using superconducting technology is approx. $100 \mu s$ [58]. In addition, gate operations can also introduce errors at rates varying between $O(10^{-3})$ for single-qubit gates and $O(10^{-2})$ for two-qubit gates. The execution time of a quantum circuit results from the aggregated time needed to run all the gates along the circuit's depth. Thus, minimizing this metric is one of the main optimizing criteria. Likewise, minimizing the total number of operations in circuits also equates to reducing the compounded error.

3 The Polyhedral Model in Quantum Computing

In this section we quickly revise the 4 polyhedral abstractions in the context of (affine) quantum circuits. We then

describe a simple domain-specific language heavily inspired in the Omega Calculator [41] and ISCC [76] notation. However, unlike its predecessors, one of its main goals is to facilitate and capture the identity schedule of the quantum circuit. We explain how the circuit structure and dependences are mapped to the polyhedral abstractions, and quickly recap well known affine loop transformations previously proposed.

3.1 Polyhedral Abstractions

Polyhedral compilers focus on fragments of programs that exhibit static control parts (SCoPs)[24–26]. From these, four abstractions are extracted: iteration domains, access functions, dependence polyhedra and scattering/scheduling functions [31].

Iteration Domains: Each syntactic statement S is associated to the set of points \mathcal{D}^S in \mathbb{Z}^+ comprised by the dynamic instances of the statement. In the context of QC, an iteration domain can group several operations of the same type or of different ones, but that behave in the same fashion. Consider for instance the `parity_247` circuit shown in Fig.1, which can be represented with two iteration domains, $\mathcal{D}^{S^1} = \{[i] : 0 \leq i < N\}$ and $\mathcal{D}^{S^2} = \{[i] : 0 \leq i < N\}$, one for the NOT operations, and another for the CNOTs; where N is an unknown but fixed value that parameterizes the circuit. We also note that several techniques have been developed to model and extend the applicability of the polyhedral model to different forms of irregular computations [6, 72, 73]. The remaining three abstractions are essentially functions applied to the iteration domains.

Program schedules: The execution order of statement instances is defined in the polyhedral model with the program schedule, a transformation matrix or an affine map that assigns to each statement instance an execution date. Schedules can be seen as multi-dimensional time-stamps

$$\Theta^S(\vec{x}) = \langle \theta_1^S, \theta_2^S, \dots, \theta_d^S \rangle, \vec{x} \in \mathcal{D}^S,$$

where θ_i^S is a one-dimensional affine function, and d is the number of dimensions in Θ^S . Schedules can be lexicographically compared, and are used in the polyhedral scanning process [9] to generate the loop structure that will visit each statement instance in the order established by the schedule Θ^S . Continuing with our ongoing example, the execution order of `parity_247` circuit can be represented with the schedules $\Theta^{S^1}(i) = \langle 0, i \rangle$, $\Theta^{S^2}(i) = \langle 1, i \rangle$. We note, however, that for this circuit loop fusion can be legally applied. In this case, another potential schedule could be $\Theta^{S^1}(i) = \langle 0, i, 0 \rangle$, $\Theta^{S^2}(i) = \langle 0, i, 1 \rangle$.

Access Relations: Are an abstraction that permit to model memory accesses. Access relations map points in an iteration domain to a data-space. The motivation is two-fold. First, to later be able to identify program statements accessing the same memory location. Second, to update the array subscript functions post-transformation. The construction

of access relations in quantum computing differs in two fundamental ways from its classical counterpart. First, in classical computing the usage of multi-dimensional arrays is the norm, whereas the current practice in quantum computing is to operate on a single, large, one-dimensional array that represents a quantum register. The second difference involves what constitutes a *read* and *write* access. In effect, in classical computing, where polyhedral compilation has been predominantly applied to imperative programming languages such as C/C++ and Fortran, there is, practically always, a single write reference and zero or more read references. This is not the case in quantum computing, where the program’s state evolves as specific entries of the register are input to gate operations. Moreover, the type of gate determines if a specific register entry is *read* or *updated*. We make this distinction for two reasons: First, some gates take control argument, which do not modify the contents of a register entry. Second, every gate operation performing a *write* also reads the input register entry, i.e. the same entry is both read and written. Resuming our example, if we assume that the top qubit has index 0, increasing downwards, then statement S2 would have three access relations, a read and write relation $\{[i] \rightarrow [0]\}$ for the target qubit, and a read-only relation $\{[i] \rightarrow [i + 1]\}$ for the control qubit.

Dependence Polyhedra embody the semantic orderings of the program. Every program dependence in a SCoP is represented by one or more dependence polyhedra $\mathcal{D}^{R \rightarrow S}$. These polyhedra define the ordering among points \vec{x}^R and \vec{y}^S from the iteration domains \mathcal{D}^R and \mathcal{D}^S , respectively. This critical pass is necessary to perform aggressive loop optimizations, and compute reordering transformations via one or more *integer linear problems* (ILPs), which must preserve the legality of the transformations applied. Essentially every scheduling technique [3, 20, 23, 28, 70] embeds the program semantic constraints in the form of dependence polyhedra (possibly linearized by the application of the Farkas Lemma) into one or more ILP systems. These polyhedra are usually extracted with “classical” data-flow dependence analysis [24].

(Parameterized) Affine Quantum Circuits (PAQCs)

We define PAQCs as a subclass of quantum programs that can be expressed with affine relations, or a union of them. We have two requirements: First, the instances of gate operations to be groupable by an affine expression; Second, the indices of qubits being accessed to be representable via affine functions.

3.2 AXL: A simple Domain-Specific Language for Parameterized Affine Quantum Circuits

Enter **AXL**, a declarative language with operations that enable the specification, manipulation and composition of quantum circuits. **AXL**’s syntax is simple and straight-forward. **AXL** provides 4 datatypes: *gate*, *circ* (constant circuits), *statement* circuits (our link to the polyhedral abstractions) and

Table 1. Quantum Gates

Gate	Description	No.Inputs	No.Outputs	Integer Map Representation
$X(rw_1)$	Pauli-X (NOT) gate	1	1	$S[\vec{x}] \rightarrow q[rw_1(\vec{x})]$
$Y(rw_1)$	Pauli-Y gate	1	1	$S[\vec{x}] \rightarrow q[rw_1(\vec{x})]$
$Z(rw_1)$	Pauli-Z gate	1	1	$S[\vec{x}] \rightarrow q[rw_1(\vec{x})]$
$H(rw_1)$	Hadamard (H) gate	1	1	$S[\vec{x}] \rightarrow q[rw_1(\vec{x})]$
$Measure(rw_1, w_2)$	Measure qubit to classical bit	1	2	$S[\vec{x}] \rightarrow q[rw_1(\vec{x})], S[\vec{x}] \rightarrow c[w_2(\vec{x})]$
$CNOT(r_1, rw_2)$	Controlled-NOT (CX)	2	1	$S[\vec{x}] \rightarrow q[r_1(\vec{x})], S[\vec{x}] \rightarrow q[rw_2(\vec{x})]$
$CY(r_1, rw_2)$	Controlled-Y	2	1	$S[\vec{x}] \rightarrow q[r_1(\vec{x})], S[\vec{x}] \rightarrow q[rw_2(\vec{x})]$
$CZ(r_1, rw_2)$	Controlled-Z	2	1	$S[\vec{x}] \rightarrow q[r_1(\vec{x})], S[\vec{x}] \rightarrow q[rw_2(\vec{x})]$
$Swap(rw_1, rw_2)$	Exchange state	2	2	$S[\vec{x}] \rightarrow q[rw_1(\vec{x})], S[\vec{x}] \rightarrow q[rw_2(\vec{x})]$
$Toffoli(r_1, r_2, rw_3)$	Controlled-Controlled-Not	2	1	$S[\vec{x}] \rightarrow q[r_1(\vec{x})], S[\vec{x}] \rightarrow q[r_2(\vec{x})], S[\vec{x}] \rightarrow q[rw_3(\vec{x})]$

program parameters. The former three define a hierarchy of types: $gates \subset circ \subset statement$. A gate is any of the operations shown in Table 1, and represents a single quantum assembly instance (or a point in \mathbb{Z}^+). The *circ* type essentially allows for the composition of gates. For example, the NOT gate operating on qubit 1 can be written as NOT(1), and a CNOT gate controlled by qubit 0 and targeting qubit 1 can be expressed as CNOT(0,1). These operations can then be synchronized (in time) via the time composition operator (+). Internally, **AXL** will manipulate the program schedule to properly represent this ordering constraint. Climbing the hierarchy we have a *circuit statement*, an enriched *circ* with polyhedral abstractions (iteration domains, access relations, gate relations, schedules). Due to space constraints, in this paper we will focus our attention on the *statement* type.

Figure 2 shows the code producing two implementations of the `parity_247` circuit in **AXL**. The first one uses a single statement (S1) to model the entire circuit, embedding both gates in its body. The (+) time-composition operator synchronizes the NOT and CNOT operations for every $t \in \mathcal{D}^{S1}$. In contrast, the second implementation puts each gate in its own statement (S2 and S3). Lines 6-7 performs code generation from each SCoP while providing non-default parameters and choosing a pre-determined transformation of choice. The second implementation imposes the synchronization of both statements also by the time-composition operator (+), which internally introduces a leading scalar dimension to their respective program schedule.

```

1 param M;
2 statement S1, S2, S3;
3 S1 := {t:1<=t<=M (%) #NOT(t) (+) #CNOT(t,0)};
4 S2 := {t:1<=t<=M (%) #NOT(t) };
5 S3 := {t:1<=t<=M (%) #CNOT(t,0)};
6 codegen {S1} with {M=8} apply {plutomax};
7 codegen {S2(+)S3} with {M=8} apply {plutomin};

```

Figure 2. AXL implementations of circuit `parity_247`

Parameterized Affine Quantum Circuits (PAQC) A unique capability of **AXL** is to represent *affine quantum circuits* in a parameterized fashion, that is, circuits can be modeled with symbolic values representing arbitrary, unknown, constant values. PAQCs are built by defining an iteration domain for the circuit and by attaching a circuit body to it. The circuit body can be: i) a basic gate; ii) a fixed, possibly composite expression of type **circ**; or iii) a parameterized, variable **circ** expression. The last of these body types, leverages the full power of the polyhedral model to represent individual instances of the computation. PAQCs are implemented in **AXL** via the **statement** type, making parameterized and variable sized quantum circuits first class citizens in our language.

We show in Table 1 a subset of the gates supported by **AXL**. The arguments to each gate represent indices in an implicit one-dimensional space; depending on the type of the gate, some arguments are either *read-only* (i.e. any r_i argument), *read-write* (arguments rw_i) or *write-only* (arguments w_k). These semantics allow us to determine the number of input and output relations, which we show in the third and fourth columns. The last column shows the extracted access relations for each of the accessed register entries, modeled as a single affine relation mapping points of the iteration domain to the data-space of the quantum register (register **q**) or of the classical register (register **c**). We follow the same naming convention to indicate when an access function is of type read, read-write or write. We note here that, although we list the main quantum gate operations, these can be quickly added into the **AXL** language under the category defined by the number of qubits, and the access type to each of its arguments.

Gate Call Relations In classical (scientific) computing, where multi-dimensional arrays are pervasive in imperative programming languages, each array reference is either read or written. This naturally follows the semantics of languages with explicit assignment operations; only the reference on the left-hand-side is written, while any array or scalar variable on the right-hand-side is read-only (except when passed to some function with side-effects). In our DSL, quantum programs operate in an implicit 1-dimensional data-space.

While there is no inherent limitation in **AXL** to represent registers in a multi-dimensional space, most quantum technologies have assumed this so far. Thus, we add a new abstraction representing *quantum gate calls*. These are very similar in spirit to classical access relations that map points in iteration domains to the various data spaces of the program. While quantum gates are effectively functions that could change the state of a register, they do come equipped with domain semantics that must be correctly mapped. More precisely, each quantum gate operation has a set of *read* and *write* index sets that establish the register entries accessed in each of these modes. Later, during the polyhedral scanning process (phase-1 of code generation) these relations are used to produce the exact quantum gate operation specified by the end-user.

Program Assembly We define **Program Assembly** as the process of constructing the final circuit schedule establishing the complete ordering among statement circuit instances in a single SCoP. It takes place at the start of the transformation and code generation process (see codegen clause in Fig.2). Building the final schedule happens in two phases. First, when defining circuit statements, a local identity schedule is created. For instance, in the same example, the local schedule $\Theta = \langle i \rangle$ is created for statements S1-S3 (Lines 3-5 in the same figure). **AXL** will then split S1 into sub-statements S1₁ and S1₂, effectively making each gate its own statement. The usage of the (+) operator for S1 will introduce a suffix scalar dimension, producing the schedules $\Theta^{S1_1} = \langle i, 0 \rangle$ and $\Theta^{S1_2} = \langle i, 1 \rangle$. The second phase of program assembly synchronizes statement circuits in a similar fashion, but with the distinction of inserting scalar dimensions as prefixes. For example, the local schedules of S2 and S3 will be modified to $\Theta^{S2} = \langle 0, i \rangle$ and $\Theta^{S3} = \langle 1, i \rangle$. Along the process, multiple scalar dimensions might be added to faithfully represent the ordering among various circuit patterns, which can be controlled by proper parenthesization.

3.3 Transformations

We next recap two well known formulations that have been extensively used at the heart of several scheduling algorithms, the Feautrier minimum latency schedules [25, 26], and the minimization of the maximal dependence distance used in the Pluto compiler [13]. In particular, Pluto has been extremely successfully in generalizing the tileability of imperfectly nested loops and using the aforementioned cost function to produce high-quality transformations. Similarly, the Feautrier algorithm has been used in [42] and is still the fallback scheduling strategy in ISL [75].

The Pluto Algorithm The Pluto Tiling Hyper-plane algorithm [13], was introduced as a general greedy algorithm to find affine transformations to make a program tileable. At its core, it uses a cost function that bounds and minimizes the distance among statements in dependence relations. As

```

1 // Plutomin (min.fusion) heuristic:
2 // Loop fission
3 for (int c1 = 1; c1 <= 8; c1 += 1) {
4   X[c1];
5 }
6 for (int c1 = 1; c1 <= 8; c1 += 1) {
7   CX[c1][0];
8 }
9 // *****
10 // Plutomax (max.fusion) heuristic:
11 // Loop fusion
12 for (int c0 = 1; c0 <= 8; c0 += 1) {
13   X[c0];
14   CX[c0][0];
15 }

```

Figure 3. Generated loop structure for circuit parity₂₄₇ using Pluto’s Minfuse and Maxfuse loop fusion heuristics

we don’t apply loop tiling to quantum programs, we only recap Pluto’s main cost function formulation below:

$$\begin{aligned}
\delta_e(\vec{x}) &= \phi_{S_i}(\vec{x}) - \phi_{S_j}(h_e(\vec{x})), \vec{x} \in P_e \\
\phi_{S_i}(\vec{x}) - \phi_{S_j}(h_e(\vec{x})) &\leq v(\vec{p}), \vec{x} \in P_e, \forall e \in E \\
v(\vec{p}) &= u \cdot \vec{p} + w \\
v(\vec{p}) - \delta_e(\vec{x}) &\geq 0, \vec{x} \in P_e, \forall e \in E \\
\text{minimize}_{<} \{u &= (u_1, u_2, u_3, \dots, u_n), \dots\}
\end{aligned}$$

The above equations essentially perform the following: i) define the constraints to satisfy a dependence edge e of the dependence set E , for every point \vec{x} in the dependence polyhedron P_e ; ii) introduce an affine function v on the vector of program parameters, \vec{p} ; iii) bound the distance between the target and source of the dependence via a function $v(\vec{p})$; iv) minimize the u coefficients that bound the dependence distance (NOTE: we omit here the application of the Farkas Lemma).

The rest of Pluto’s algorithm proceeds level-by-level, from the outermost to the innermost, finding one-dimensional affine transforms for all statements in the program. By default, *splitters* (scalar dimensions) are only introduced by the algorithm when no solutions are found for a new hyperplane. However, doing this whenever is legal, produces loop structures maximally distributed. We show in Fig.3 the result of applying both heuristics, labelled as *Plutomin* and *Plutomax*, to the **AXL** implementation of the parity₂₄₇ circuit.

The Feautrier Scheduling Algorithm Feautrier’s seminal papers [25, 26] on one-dimensional and multi dimensional affine schedules have been a common test for several applications and domains. The main property of Feautrier’s

Table 2. Geometric Mean Circuit Depth and Added Gates across topologies, loop transformations and qubit allocators

Topology x Transformation	Circuit Depth (No.Gates)				No. of Added Gates			
	jku	ibm	sabre	wpm	jku	ibm	sabre	wpm
multi-ring x base	204.79	314.63	208.17	358.02	317.25	568.47	290.30	723.47
multi-ring x feautrier	211.31	311.54	203.04	358.47	327.48	556.27	275.04	747.09
multi-ring x plutomin	203.85	312.80	204.96	367.19	316.87	562.75	269.52	769.92
multi-ring x plutomax	206.43	309.15	205.16	356.87	321.21	550.15	284.55	735.11
grid x base	162.31	228.26	169.33	307.15	225.17	419.21	203.31	584.08
grid x feautrier	167.22	225.93	169.20	302.71	249.83	417.37	226.35	626.60
grid x plutomin	161.93	228.69	165.52	308.05	225.12	425.11	208.55	626.09
grid x plutomax	161.61	228.71	170.60	298.12	224.40	415.32	223.36	590.60
tilted x base	191.55	250.50	198.37	319.59	336.20	469.33	288.63	370.72
tilted x feautrier	196.23	254.10	192.31	321.07	344.30	473.35	294.37	385.64
tilted x plutomin	190.22	249.75	188.44	315.98	330.93	473.35	266.59	382.62
tilted x plutomax	195.73	246.92	194.65	329.98	333.47	461.80	287.61	379.69

scheduling approach is to greedily satisfy as many dependences as early as possible, going from the outermost (linear) dimension to the innermost. This greedy approach produces schedules with the minimum number of dimensions. More importantly, this approach yields the maximum freedom to reorder operations in the innermost loop dimensions.

4 Experimental Evaluation

We have implemented the **AXL** language, and the analyses and transformations described in Section 3 as a source-to-source compiler toolchain using the Integer Set Library [75]. Quantum circuits are written and compiled with **AXL** to produce the loop structure, which is then post-processed to construct a compilable C-program. This is then compiled into an executable binary to finally generate the stream of quantum assembly operations, targeting either the ProjectQ [67] compiler or OpenQASM 2.0 [21]. In particular, the results shown here are obtained with QASM files. The **AXL** benchmarks were compiled on an 8-core AMD Ryzen 7 2700X - 2.1GHz with 105GB DRAM, 32KB L1, 512KB L2 and 8MB L3 cache.

The overall goal of our experimental evaluation is to demonstrate that even “classical” high-level loop transformations, i.e. not yet tailored to the quantum computing domain, can synergistically work with back-end compiler optimization such as Qubit Allocation. Thus, our goal is to determine where (in which experimental configurations), why (interactions of loop transformations with the qubit allocator) and when (in some specific stage of a circuit) can impact the qubit allocation result, either for good (improved quality, i.e. shallower circuits) or bad (bigger circuits).

Testbed and Protocol: We use the Enfield compiler [1, 2], which implements several qubit allocation techniques. In particular, we consider four of the qubit allocation algorithms covered in Sec.2: *sabre* [48], *jku* [81], *wpm* [62], and *ibm* [37]. Enfield allows to collect statistics such as allocation time, circuit depth (no. of gates in critical path), circuit

size (total no. of gates) among many others. The methodology we follow is the same as that of **sabre** [48] when comparing against **jku**, while **wpm** and **jku** compare against the **ibm** mapper in their respective publications. As context, the **jku** paper reported a 23% improvement (no. of elementary gates added) w.r.t. to **ibm**, while **sabre** reports an average improvement of 14% over **jku**, considering their qft and large benchmark categories.

We use the circuit depth and size as primary quality metrics, which vary with the allocator due to the number of *quantum SWAP* and *REVERSE* operations introduced to advance the program state, usually between adjacent layers. Each of these operations is implemented with elementary gates. Each SWAP is implemented with 3 CNOT, while each reverse operation requires 4 Hadamard (H) and 1 CNOT gates.

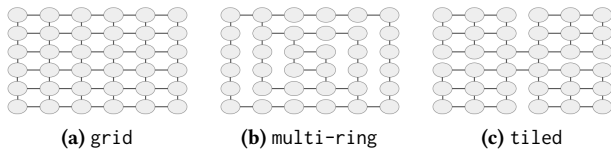
Our experimental testbed consists of the eight quantum circuits listed in Table 3, which were taken from the literature². We generate four different variants for each benchmark: pass-through mode performing only code generation (*base*); the transformed code obtained by applying the Feautrier scheduling algorithm (*feautrier*) [25, 26]; and the two well known Pluto’s fusion heuristics, maximal loop fusion (*plutomax*) and maximal loop distribution (*plutomin*). We note that the *base* variant, while only involving code generation, can already be considered an optimized program, as the polyhedral scanning process will produce minimal control overhead that can vastly differ from hand-written loop-based code [9]. The latter two variants represent ends of the classical locality spectrum. Although Enfield already repeats the allocation process for the algorithms with random properties (5 for **sabre** and 20 for **ibm**), we still found substantial variation in the results. Thus, for each allocator we repeat the allocation process 10 times and report their arithmetic mean. We also include error bars showing the standard deviation.

²Please refer to the Appendix for a larger **AXL** example and circuit diagrams

Table 3. Quantum Circuits Evaluated with Default Parameters

Benchmark Name	Source	No.State-ments	No.Polyhedral Dependences	Para-meters	No.Qubits	No.QASM ops	Output Lines
adder-maj-uma	[22]	3	11	N=9	20	55	13-15
cuccaro-adder-6bit	[22]	6	50	N=6	14	46	26-36
sum5	[69]	7	41	N=5	11	36	22-32
init-G ₅	[69]	8	33	N=5	11	35	24-34
cheung	[17]	1	1	N=6	18	21	5
pipelined-swap	[27]	13	28	N=6	14	75	37-43
cnt3-5_179	[79]	2	14	N=5	19	30	14-20
rd84_142	[79]	3	36	M=2, N=4	15	28	16-32

Evaluated Topologies: Just as in classical computing the underlying architecture (e.g. multi-core CPU, many-core CPU, GPUs, etc) can have a substantial impact on the program’s performance, in quantum computing the quality of the resulting qubit allocation can depend of the underlying architecture (topology). We thus evaluate three coupling graphs with the same number of qubits (36), and slightly vary the graph’s connectivity to produce different properties. The three coupling graphs used are shown in Fig.4, and include a 6×6 grid (grid), a graph with three doubly-linked concentric rings (multi-ring), and a four 3×3 tiled array of qubits (tiled). All graphs have the same diameter (10), but differ in their bisection bandwidth, which is 6 for multi-ring and grid, and only 2 for tiled. In addition, having more qubits with higher degree enhances the architectural parallelism. For instance, if a given qubit has degree d , then completing an update (write) on this qubit can enable up to $d - 1$ gate-to-gate dependences. For multi-ring, tiled and grid the number of gates with degree 3 or greater are 8, 24 and 32, respectively. This design decision differs from the IBM QX20 (Tokyo) coupling graph, which varies over time, and which typically has several qubits with degree 5 or 6.

**Figure 4.** Evaluated coupling graphs (topologies)

TL;DR: Overall, we observe that quantum qubit allocation algorithms and quantum programs can benefit from the power of global cost functions offered by polyhedral optimization techniques. Our evaluation shows that even the most advanced allocators (**jku** and **sabre**) can improve up to 34%, while achieving 60% on **wpm**. We also observe and confirm general trends such as allocation variability due to the inherent data- and pipelined- parallelism, distance among qubit operands, or the hardware parallelism available.

General Trends We summarize in Tab.2 the geometric mean of the circuit depth (no.gates) and number of added gates across all combinations of topologies, affine transformations and qubit allocators. The first trend to observe is that the depth of the circuit tends to increase with lower architectural parallelism (e.g. no. of qubits with degree 3 or greater), as expected. Next, we observe that even the state-of-the-art allocators, **jku** and **sabre**, can greatly benefit from affine transformations. In particular, we observe up to a 10% gap of added gates ($\max \Delta_{transform} / \max(added)$) due to loop transformations in the {grid,**jku**}, {grid,**sabre**} and {tiled,**sabre**} configurations. In regard to **jku**, this qubit allocator produces the shortest circuits (depth-wise) in all three topologies when used in combination with *plutomin*, and producing its worst circuit depth when combining it with *feautrier*. This trend is nearly the same for **sabre**. Lastly, we don’t observe any obvious trend involving the **ibm** allocator.

In regard to the number of gates added by each allocator (last 4 columns), we observe that this metric also correlates with the architectural parallelism of the topologies used. We also observe that an overall increase of gate count does not necessarily correlate with better circuit depth. This phenomenon can be seen when comparing the {grid,**jku**} and {grid,**sabre**} with {multi-ring,**jku**} and {multi-ring,**sabre**}.

Individual Analysis with Default Parameters We next dissect the behavior of our eight quantum circuits, and show the achieved circuit depth in Fig.5. For each circuit, we cluster the results by topology × allocator. Each bar represents the mean of 10 repetitions, and include their corresponding standard deviation. In addition, each cluster is also tagged with the highest percentual variation between the highest and lowest depth ($(depth_{max} - depth_{min}) / depth_{max}$) among the loop transformation for the same topology and allocator. In general, we expect lower variation for the grid topology than for the multi-ring and tiled topologies.

Turning our attention to the pipelined-swap circuit. This benchmark represents the swap between two distant qubits

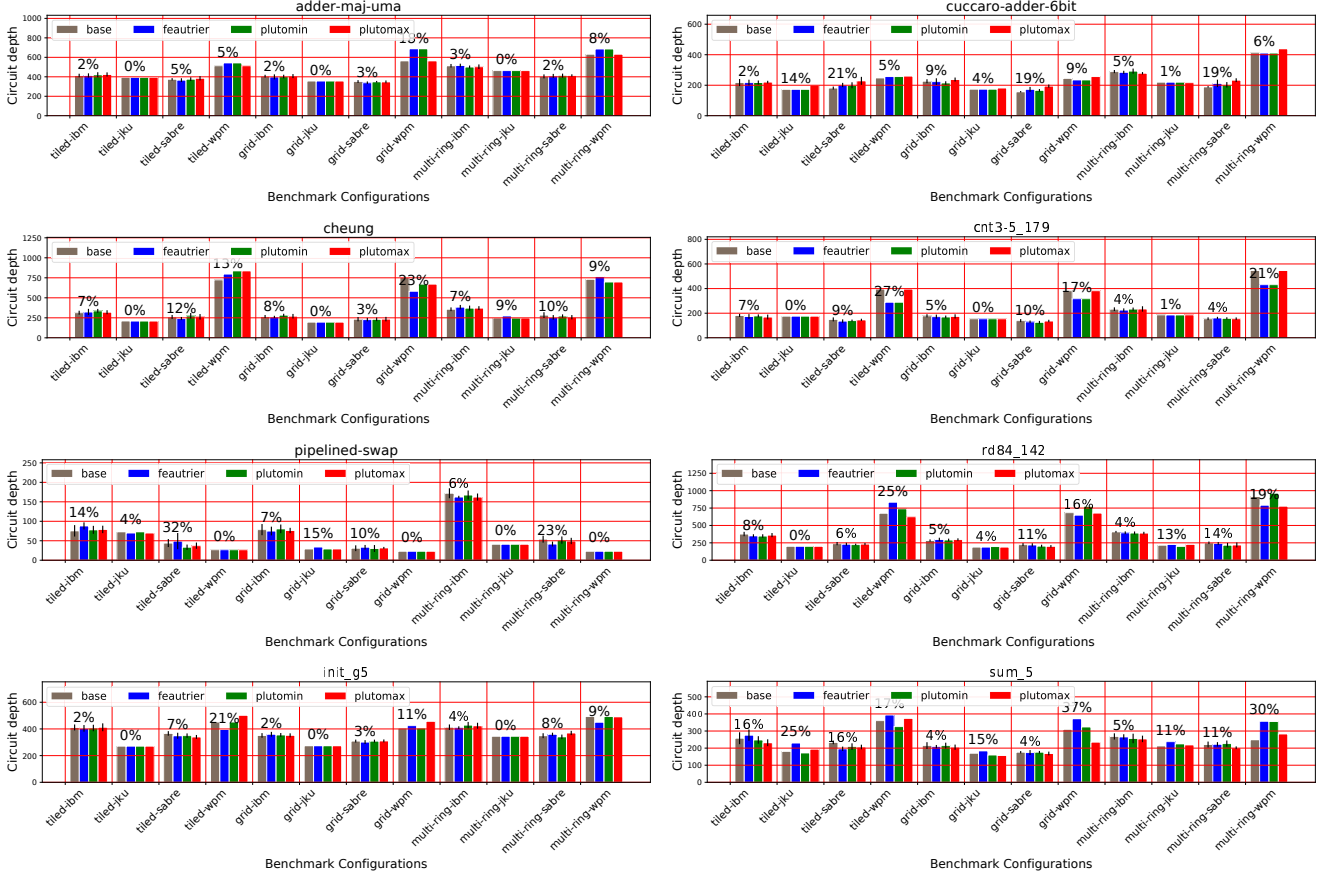


Figure 5. Impact of Affine Loop Transformations on circuit depth for grid, multi-ring and tiled

(e.g. q_0 and q_{35}). The circuit initially exhibits 2-way parallelism, simultaneously starting with the two qubits, and morphing into pipelined parallelism in its steady-state (See Appendix for circuit diagram). Each CNOT operation being the input dependence to the operations on two adjacent qubits. The interesting result here is that **wpm**, which typically produces lower quality mappings, consistently produces shallower circuits. We also observe up to a 23% gap for **sabre** on the multi-ring topology yielded by the *feautrier* transformation.

The cheung circuit exhibits N-way data-parallelism, N being the number of pipelined CCNOT (Controlled-Controlled NOT) gates found at the bottom of the circuit. The first CCNOT of each qubit can be mapped to a distinct qubit to maximize parallelism and reduce the circuit depth. Intuitively, both the *feautrier* and *plutomax* should yield the highest benefit in terms of circuit depth, since maximizing the number of satisfied dependences per schedule dimension equates (for this benchmark) to minimizing the maximal-dependence distance. The circuit's depth drastically increases with the quality of the qubit allocator. This is due to the fact that the

control qubits for each operation start the closest and separate as the state evolves. This, in turn, requires more swaps operations to make the qubit operands adjacent.

The arithmetic adder using the majority and unmajority circuit pattern, adder-maj-uma, exhibits a highly serial form in its steady-state. The only opportunities for reordering transformations arise from the potential fusion/distribution of the CNOT operations with the sequence of CCNOTs following later. In general terms, we expect the *plutomax* to have the highest impact on the circuit depth. The same observations hold for the cuccaro-adder-6bit adder, which differs from the former in the degree of data-parallelism. This translates to much shallower circuits, roughly half the depth of the adder-maj-uma counterparts. It also differs in that *base* and *plutomin* typically achieve the best circuit depth due to the already available parallelism. All four qubit allocators also benefit from the higher scheduling and placement flexibility of cuccaro-adder-6bit due to the lower number of CCNOTs (3-operand gates) as well as the presence of CNOT and NOT gates.

Benchmarks sum5 and init-G₅ [69] share similar properties. As both exhibit distinct and noticeable parallel and

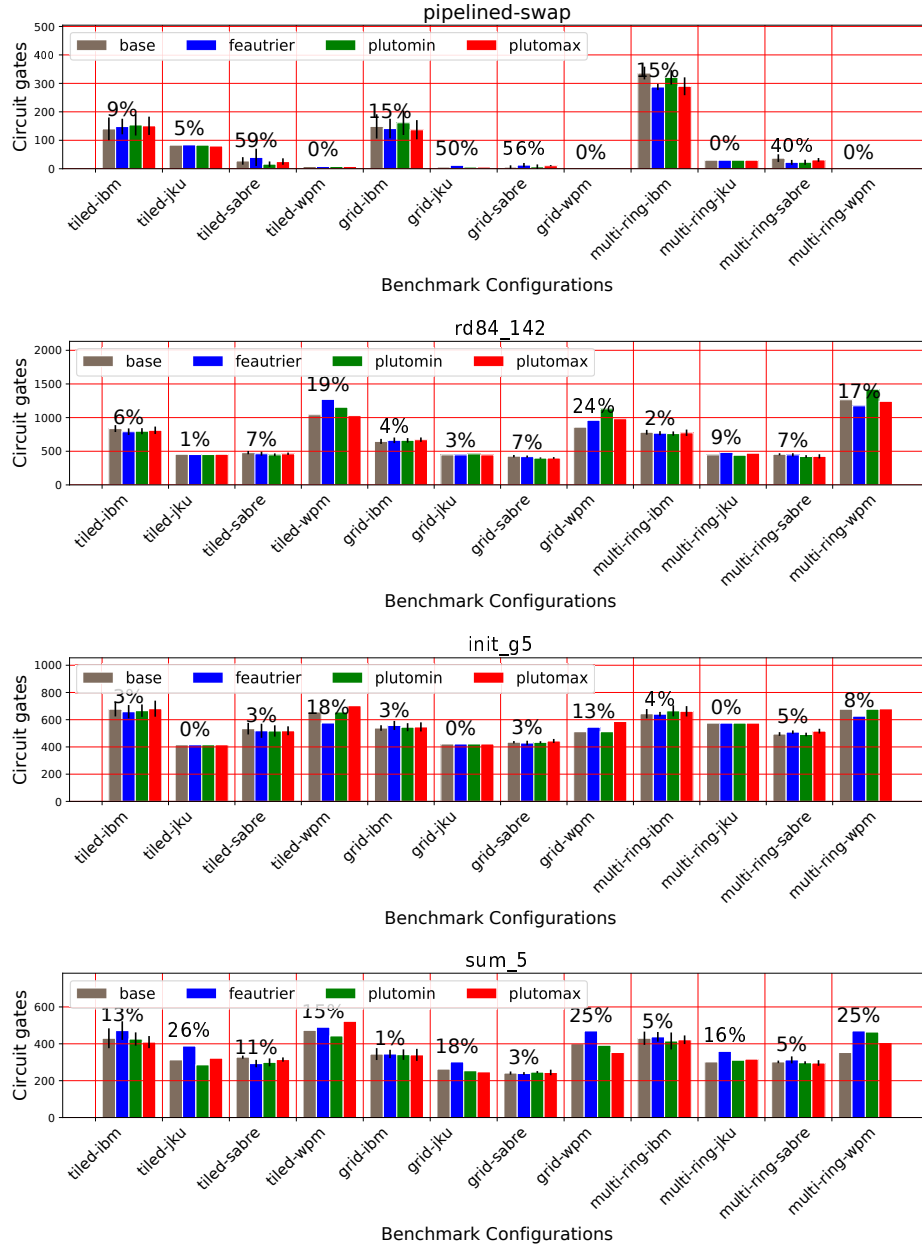


Figure 6. Impact of Affine Loop Transformations on circuit size for grid, multi-ring and tiled

serial phases. For instance, `sum5`'s initial and `init-G5` ending phase offer a lot of reordering freedom in the scheduling and placement of the CNOT operations. In contrast, the middle and ending phases of `sum5` and initial and middle ones of `init-G5` are mostly serial with stints of pipelined parallelism. In addition, the large and varying separation between the gate operands induce a higher number of required SWAP operations. These combination of factors make harder the prediction of the most suitable affine transformation, making the outcome highly variable w.r.t to the coupling

graph and the qubit allocator. So the overall topological trends remain.

Circuit `cnt3-5_179` also shares some similar features with circuit `cuccaro-adder-6bit`. They both have a mix of data- and pipelined parallelism, with short constant distance (3 or lower) among the gate operands. These traits contrast with benchmark `rd84_142` which exhibits much larger, but constant separation (5). `cnt3-5_179` benefits from a slighter higher degree of data parallelism (left-most CNOTs). Given the combination of characteristics, we expect *plutomax* to

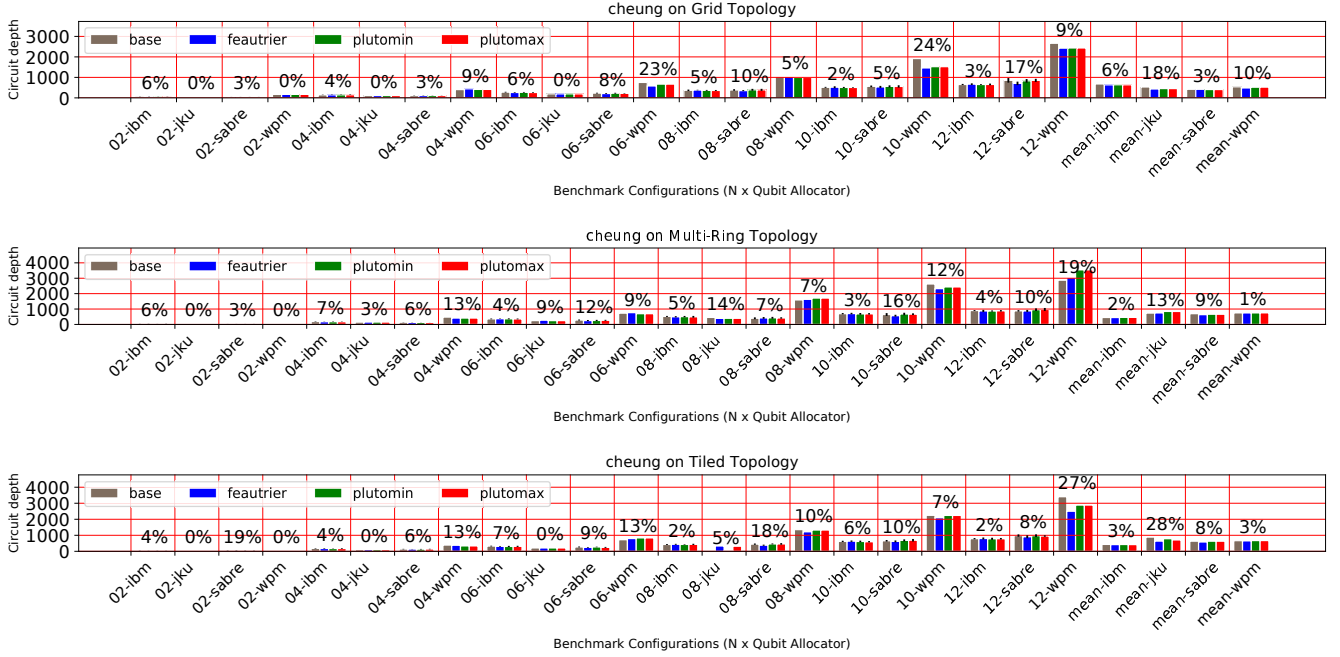


Figure 7. Impact of problem size scaling on circuit depth for cheung circuit on topologies grid (top), multi-ring (middle) and tiled (bottom)

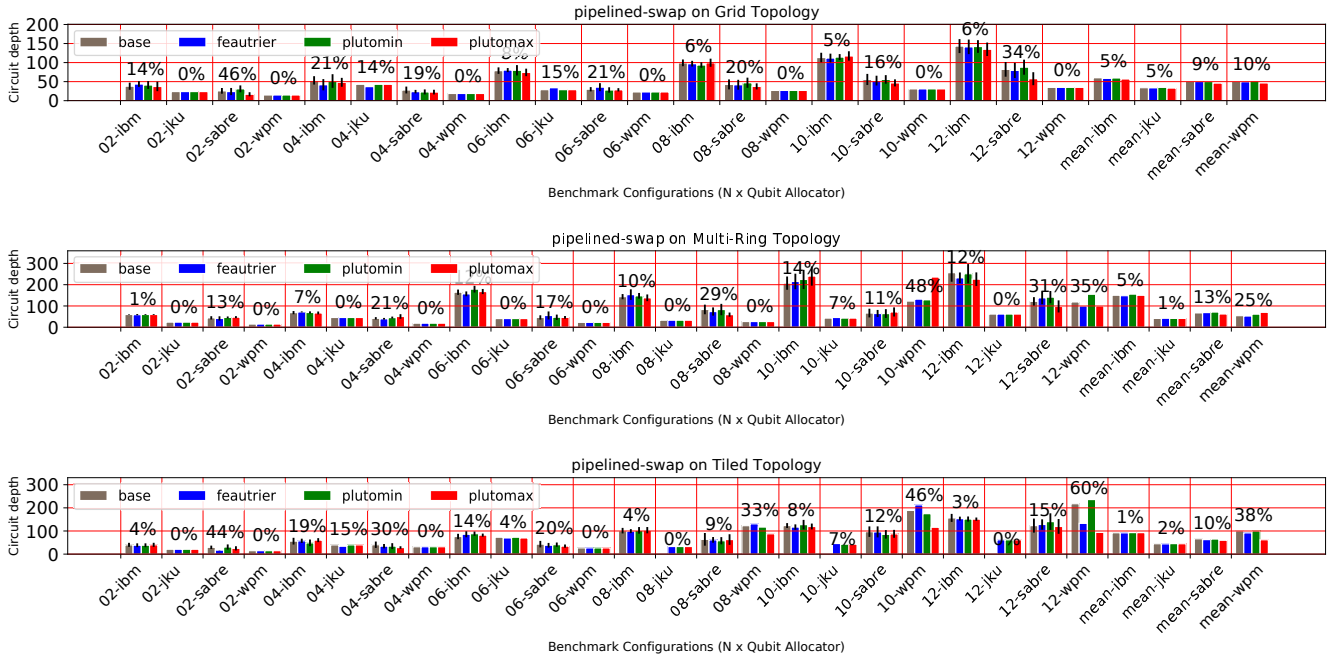


Figure 8. Impact of problem size scaling on circuit depth for pipelined-swap circuit on topologies grid (top), multi-ring (middle) and tiled (bottom)

be more beneficial for rd84_142, while *feautrier* and *plutomin* to perform best (or close to) for cnt3-5_179, as loop fission will effectively isolate the parallel operations from

the more serial/pipelined ones. Empirically, both of these observations and hypotheses hold.

Impact on Circuit Size Next, we show in Fig.6 the gap in circuit size for four of the previous circuits. The analysis and justification is as before, revolving around the variability in data- and pipelined parallelism, specific properties of the circuits such as the distance between its qubit operands (fixed-short, fixed-large or variable), and the underlying topology. In particular, we highlight that **wpm** effectively detected that the **pipelined-swap** was a swap circuit in itself, unlike all other allocators, which still attempted to optimize the circuit. We also observe circuit gaps ($\max \Delta_{transform} / \max(added)$) of up to 26% even for **jku**, on `sum5`.

Impact of Circuit Scaling To complement our study, we perform a scaling evaluation of circuits `pipelined-swap` and `cheung`. We focus on these benchmarks due to their high regularity and lack of singleton quantum statements that require more specific scheduling. We vary the SCoP parameter $N \in \{2..12\}$. Beyond this, the quantum register size is exceeded. To judge the overall scaling behavior, the last four bar clusters in each figure show the arithmetic mean of each allocator varying the loop transformation. We note that `pipelined-swap` using **jku** on the grid topology only scaled up to $N=6$ (14 qubits), at which point each run started taking above an hour to complete. Furthermore, at $N=10$, memory was being exhausted in our benchmarking server. The time limit was also exceeded for the *base* variant of `pipelined-swap` using **jku** on the other two topologies, for $N \geq 8$. A consequence of the A^* search used by **jku**. Next, we center our attention on the `cheung` benchmark, which only utilizes CCNOT gates. This trait makes it fare best on topologies with higher number of vertices with degree 3 or higher, i.e. `tilled` (24) and `grid` (32). The impact of this requirement is notorious on the `multi-ring` (8) graph, which for $N=4$ requires a total of 8 (4 producing and 4 consuming) gates. Past this point the number of swaps operations introduced by the **wpm** allocator nearly doubles for every increment of 2 on N . Given these resource restrictions, we now refine our first assessment on this circuit, and expect the *feautrier* transformation to fare best, as it was conceived as a minimum latency, resource conscious transformation. Equivalently, we also now expect *plutomax* to induce typically higher circuit depth. The intuition here (in classical loop transformation terms) is that the *plutomax* heuristic would amount to an outer parallel loop and an inner serial loop, while the *feautrier* transformation would make the outer loop serial, thereby exposing more inner parallelism. The general effect of this trade-off for most qubit allocators is to expose earlier the gate-to-gate dependences. In particular, this is most beneficial when the allocator makes local decisions using sliding windows.

Changing our focus to the `pipelined-swap` circuit, we first note that, unlike the previous benchmark, this one only consists of CNOT gates. Thus, the number of vertices with degree 3 or higher is not a limiting factor. This provides

more freedom to the qubit allocators. In general, the **jku** allocator produces the circuits with the shallowest depth, outperforming **sabre** in every topology. Nonetheless, we highlight that **wpm** in tandem with *plutomax* yields results comparable, and at times better, than **sabre**. This is relevant because **wpm** is $10\times$ faster than **sabre** and $10\times$ to $15\times$ faster than **jku**. The much improved circuit depth w.r.t to **wpm**'s impact on other benchmarks is due to a specific feature of `pipelined-swap`. If we divide the circuit into four quadrants, the north-east (NE), north-west (NW), south-east (SE) and south-west (SW), and consider them as the four statements to schedule, we can notice that the NW and SW statements converge in the middle of the circuit. This means that the underlying qubit allocator would benefit from finding those operations, the ones in the middle of the four quadrants, concentrated into a small window of operations. That is precisely the effect of using *plutomax*, and leads up to a 60% circuit depth improvement when using **wpm** on the `tilled` topology.

5 Related Work

Modeling affine quantum circuits shares some similarities with polyhedral process networks (PPN) [54, 74], independent processes that communicate with unbounded FIFOs. However, most of their work has focused on translating serial programs into parallel hardware. Polyhedral and affine transformations have also successfully targeted several architectures, among them CPUs [38, 49], GPUs [8, 32, 47, 77], and FPGAs [4, 57]. Functional languages have been proposed as viable candidates for the specification of quantum programs: [46] introduced a statically typed functional DSL; [5] introduced the QML language focused on allowing the specification of reversible and irreversible quantum computations and combining it with first order strict linear logic. The Scaffold language and the Scaffold compiler [39, 40] allow for a modular organization of quantum programs, and are equipped with control-flow constructs that allow to manipulate quantum gates. Loke, Wang and Chen [16, 50] developed the Qcompiler and OptQC, which focused on the optimization of circuits by determining permutation matrices that minimized the number of required swap gates. Their algorithm used simulated annealing to determine near optimal number of swap gates. Svore et al. developed Q# [68], a DSL with a rich type system, modular definitions, reversible operations, control-flow constructs and qubit management. Similarly, quantum instructions sets [63] and assembly languages such as OpenQASM [21] and cQASM [12] (the common Quantum Assembly language) have also been proposed. QISKit [37] is an open sourced quantum toolkit, available as a Python package, which enables users to write programs with OpenQASM and run them in the IBM Quantum Experience [58], a cloud service. These efforts embody important software building blocks that new quantum compiler

infrastructures can build upon to develop more scalable and high-level frameworks. RevKit [64, 65] has also been used to support fully automatic synthesis of quantum circuits [66]. Quipper [29, 30], an embedded quantum programming language for circuit specification developed by Green et al., introduced several features such as ancilla scope and reuse, classical to quantum circuit lifting for automatic generation of application specific oracles, basic data types, boxed/procedural definition and reversing operators for defined circuits. LIQW [78], a DSL for quantum computing, proposed language features such as static typing, opaque types for qubit and kets representation, and introspection functionality that uses Microsoft’s F# language and .NET support. [55] introduced QWIRE, a language designed for the specification of quantum circuits with strong type system and safe properties for well defined circuits. In QWIRE, circuits are first-class citizens, and provides boxing and unboxing functionality that enables the composition of circuits. In addition, it also leverages dynamic lifting to convert a quantum circuit to its classical equivalent. Lastly, efforts to produce more robust quantum program mappings for NISQ (Noisy Intermediate-Scale Quantum) architectures by exploiting calibration parameters, scalability and routing options are also being explored [53].

6 Conclusion and Future Directions

In this paper we have introduced the first polyhedral quantum specification language and compiler, **AXL**. We have demonstrated how off-the-shelf polyhedral analyses and transformations from the classical HPC world can be applied and beneficial to quantum computing. We have found that even not-yet-tailored transformations can improve state-of-the-art qubit allocators such as **jku** and **sabre** by as much as 36%, and others such as **wpm** by 60%. Clearly, much work remains. An obvious follow up is to devise different model-driven optimizations that embed parallelism constraints, as well as considering the underlying machine topology.

References

- [1] [n. d.]. Enfield. ([n. d.]). <https://github.com/ysiraichi/enfield.git> Online; accessed on August 2020.
- [2] [n. d.]. Qubit Allocation: The Enfield Project. ([n. d.]). <http://cuda.dcc.ufmg.br/enfield/> Online; accessed on August 2020.
- [3] Aravind Acharya, Uday Bondhugula, and Albert Cohen. 2018. Polyhedral Auto-transformation with No Integer Linear Programming. In *Proceedings of the 39th ACM SIGPLAN Conference on Programming Language Design and Implementation (PLDI 2018)*. ACM, New York, NY, USA, 529–542. <https://doi.org/10.1145/3192366.3192401>
- [4] C. Alias, A. Darte, and A. Plesco. 2013. Optimizing remote accesses for offloaded kernels: Application to high-level synthesis for FPGA. In *2013 Design, Automation Test in Europe Conference Exhibition (DATE)*. 575–580.
- [5] Thorsten Altenkirch and Jonathan Grattage. 2005. A functional quantum programming language. In *Logic in Computer Science, 2005. LICS 2005. Proceedings. 20th Annual IEEE Symposium on*. IEEE, 249–258.
- [6] Travis Augustine, Janarthanan Sarma, Louis-Noël Pouchet, and Gabriel Rodríguez. 2019. Generating Piecewise-regular Code from Irregular Structures. In *Proceedings of the 40th ACM SIGPLAN Conference on Programming Language Design and Implementation (PLDI 2019)*. ACM, New York, NY, USA, 625–639. <https://doi.org/10.1145/3314221.3314615>
- [7] Adriano Barenco, Artur Ekert, Kalle-Antti Suominen, and Päivi Törmä. 1996. Approximate quantum Fourier transform and decoherence. *Physical Review A* 54, 1 (1996), 139.
- [8] Muthu Manikandan Baskaran, Uday Bondhugula, Sriram Krishnamoorthy, J. Ramanujam, Atanas Rountev, and P. Sadayappan. 2008. A Compiler Framework for Optimization of Affine Loop Nests for Gpgpus. In *Proceedings of the 22Nd Annual International Conference on Supercomputing (ICS ’08)*. ACM, New York, NY, USA, 225–234. <https://doi.org/10.1145/1375527.1375562>
- [9] Cedric Bastoul. 2004. Code generation in the polyhedral model is easier than you think. In *Proceedings. 13th International Conference on Parallel Architecture and Compilation Techniques, 2004. PACT 2004*. 7–16. <https://doi.org/10.1109/PACT.2004.1342537>
- [10] Stephane Beauregard. 2002. Circuit for Shor’s algorithm using $2n+3$ qubits. *arXiv preprint quant-ph/0205095* (2002).
- [11] Benjamin Bichsel, Maximilian Baader, Timon Gehr, and Martin Vechev. 2020. Silq: A High-Level Quantum Language with Safe Uncomputation and Intuitive Semantics. In *Proceedings of the 41st ACM SIGPLAN Conference on Programming Language Design and Implementation (PLDI 2020)*. Association for Computing Machinery, New York, NY, USA, 286–300. <https://doi.org/10.1145/3385412.3386007>
- [12] Lev S Bishop. 2017. Qasm 2.0: A quantum circuit intermediate representation. In *APS Meeting Abstracts*.
- [13] Uday Bondhugula, Albert Hartono, J. Ramanujam, and P. Sadayappan. 2008. A Practical Automatic Polyhedral Parallelizer and Locality Optimizer. In *Proceedings of the 29th ACM SIGPLAN Conference on Programming Language Design and Implementation (PLDI ’08)*. ACM, New York, NY, USA, 101–113. <https://doi.org/10.1145/1375581.1375595>
- [14] Michel Boyer, Gilles Brassard, Peter Høyer, and Alain Tapp. 1998. Tight bounds on quantum searching. *Fortschritte der Physik: Progress of Physics* 46, 4-5 (1998), 493–505.
- [15] G. J. Chaitin. 1982. Register Allocation & Spilling via Graph Coloring. In *Proceedings of the 1982 SIGPLAN Symposium on Compiler Construction (SIGPLAN ’82)*. Association for Computing Machinery, New York, NY, USA, 98–105. <https://doi.org/10.1145/800230.806984>
- [16] YG Chen and JB Wang. 2013. Qcompiler: Quantum compilation with the CSD method. *Computer Physics Communications* 184, 3 (2013), 853–865.
- [17] Donny Cheung, Dmitri Maslov, Jimson Mathew, and Dhiraj K Pradhan. 2008. On the design and optimization of a quantum polynomial-time attack on elliptic curve cryptography. In *Workshop on Quantum Computation, Communication, and Cryptography*. Springer, 96–104.
- [18] Je a Chilverini, J Britton, D Leibfried, E Knill, Murray D Barrett, RB Blakestad, Wayne M Itano, John D Jost, C Langer, R Ozeri, et al. 2005. Implementation of the semiclassical quantum Fourier transform in a scalable system. *science* 308, 5724 (2005), 997–1000.
- [19] Richard Cleve and John Watrous. 2000. Fast parallel circuits for the quantum Fourier transform. In *Foundations of Computer Science, 2000. Proceedings. 41st Annual Symposium on*. IEEE, 526–536.
- [20] Albert Cohen, Marc Sigler, Sylvain Girbal, Olivier Temam, David Parrello, and Nicolas Vasilache. 2005. Facilitating the search for compositions of program transformations. In *Proceedings of the 19th annual international conference on Supercomputing*. ACM, 151–160.
- [21] Andrew W Cross, Lev S Bishop, John A Smolin, and Jay M Gambetta. 2017. Open quantum assembly language. *arXiv preprint arXiv:1707.03429* (2017).
- [22] Steven A Cuccaro, Thomas G Draper, Samuel A Kutin, and David Petrie Moulton. 2004. A new quantum ripple-carry addition circuit. *arXiv preprint quant-ph/0410184* (2004).

- [23] Paul Feautrier. 1988. Parametric integer programming. *RAIRO-Operations Research* 22, 3 (1988), 243–268.
- [24] Paul Feautrier. 1991. Dataflow analysis of array and scalar references. *International Journal of Parallel Programming* 20, 1 (01 Feb 1991), 23–53. <https://doi.org/10.1007/BF01407931>
- [25] Paul Feautrier. 1992. Some efficient solutions to the affine scheduling problem. I. One-dimensional time. *International Journal of Parallel Programming* 21, 5 (01 Oct 1992), 313–347. <https://doi.org/10.1007/BF01407835>
- [26] Paul Feautrier. 1992. Some efficient solutions to the affine scheduling problem. Part II. Multidimensional time. *International journal of parallel programming* 21, 6 (1992), 389–420.
- [27] Craig Gidney. 2017. Algorithmic Assertions: Breaking Down the Quantum Swap. (2017). <https://algassert.com/post/1717>
- [28] Sylvain Girbal, Nicolas Vasilache, Cédric Bastoul, Albert Cohen, David Parello, Marc Sigler, and Olivier Temam. 2006. Semi-automatic composition of loop transformations for deep parallelism and memory hierarchies. *International Journal of Parallel Programming* 34, 3 (2006), 261–317.
- [29] Alexander S Green, Peter LeFanu Lumsdaine, Neil J Ross, Peter Selinger, and Benoît Valiron. 2013. An introduction to quantum programming in quipper. In *International Conference on Reversible Computation*. Springer, 110–124.
- [30] Alexander S. Green, Peter LeFanu Lumsdaine, Neil J. Ross, Peter Selinger, and Benoît Valiron. 2013. Quipper: A Scalable Quantum Programming Language. In *Proceedings of the 34th ACM SIGPLAN Conference on Programming Language Design and Implementation (PLDI '13)*. ACM, New York, NY, USA, 333–342. <https://doi.org/10.1145/2491956.2462177>
- [31] Martin Griebl, Paul Feautrier, and Christian Lengauer. 2000. Index Set Splitting. *Int. J. Parallel Program.* 28, 6 (2000), 607–631. <https://doi.org/10.1023/A:1007516818651>
- [32] Tobias Grosser and Torsten Hoefler. 2016. Polly-ACC Transparent Compilation to Heterogeneous Hardware. In *Proceedings of the 2016 International Conference on Supercomputing (ICS '16)*. ACM, New York, NY, USA, Article 1, 13 pages. <https://doi.org/10.1145/2925426.2926286>
- [33] Lov K Grover. 1996. A fast quantum mechanical algorithm for database search. In *Proceedings of the twenty-eighth annual ACM symposium on Theory of computing*. ACM, 212–219.
- [34] Lisa Hales and Sean Hallgren. 2000. An improved quantum Fourier transform algorithm and applications. In *Foundations of Computer Science, 2000. Proceedings. 41st Annual Symposium on*. IEEE, 515–525.
- [35] P. E. Hart, N. J. Nilsson, and B. Raphael. 1968. A Formal Basis for the Heuristic Determination of Minimum Cost Paths. *IEEE Transactions on Systems Science and Cybernetics* 4, 2 (1968), 100–107.
- [36] Jeff Heckey, Shruti Patil, Ali JavadiAbhari, Adam Holmes, Daniel Kudrow, Kenneth R Brown, Diana Franklin, Frederic T Chong, and Margaret Martonosi. 2015. Compiler management of communication and parallelism for quantum computation. *ACM SIGARCH Computer Architecture News* 43, 1 (2015), 445–456.
- [37] IBM-Research, Alexandre Blais, Robin Blume Kohout, Francesco Buscemi, Jonas Bylander, Isaac Chuang, Vincent Dwyer, Mark Everitt, Michael Geller, Thomas Haener, Andrew Houck, Thomas Ihn, Sabre Kais, Miguel Ángel Martín-Delgado, Rod Van Meter, Harumichi Nishimura, Russell Rundel, Enrique Solano, Damian Steiger, Todd Tilma, Christophe Vuillot, Martin Weides, James Wootton, and Shigeru Yamashita. 2018. Open Source Quantum Information Science Kit. (2018). <https://qiskit.org>
- [38] F. Irigoin and R. Triolet. 1988. Supernode Partitioning. In *Proceedings of the 15th ACM SIGPLAN-SIGACT Symposium on Principles of Programming Languages (POPL '88)*. ACM, New York, NY, USA, 319–329. <https://doi.org/10.1145/73560.73588>
- [39] Ali JavadiAbhari, Arvin Faruque, Mohammad J Dousti, Lukas Svec, Oana Catu, Amlan Chakrabati, Chen-Fu Chiang, Seth Vanderwilt, John Black, and Fred Chong. 2012. *Scaffold: Quantum programming language*. Technical Report. PRINCETON UNIV NJ DEPT OF COMPUTER SCIENCE.
- [40] Ali JavadiAbhari, Shruti Patil, Daniel Kudrow, Jeff Heckey, Alexey Lvov, Frederic T Chong, and Margaret Martonosi. 2015. Scaffold: Scalable compilation and analysis of quantum programs. *Parallel Comput.* 45 (2015), 2–17.
- [41] Wayne Kelly, Vadim Maslov, William Pugh, Evan Rosser, Tatiana Shepman, and Dave Wonnacott. 1996. The Omega calculator and library, version 1.1. 0. *College Park, MD 20742* (1996), 18.
- [42] Martin Kong, Richard Veras, Kevin Stock, Franz Franchetti, Louis-Noël Pouchet, and P. Sadayappan. 2013. When Polyhedral Transformations Meet SIMD Code Generation. In *Proceedings of the 34th ACM SIGPLAN Conference on Programming Language Design and Implementation (PLDI '13)*. ACM, New York, NY, USA, 127–138. <https://doi.org/10.1145/2491956.2462187>
- [43] PG Kwiat, JR Mitchell, PDD Schwindt, and AG White. 2000. Grover's search algorithm: an optical approach. *Journal of Modern Optics* 47, 2-3 (2000), 257–266.
- [44] Thaddeus D Ladd, Fedor Jelezko, Raymond Laflamme, Yasunobu Nakamura, Christopher Monroe, and Jeremy Lloyd O'Brien. 2010. Quantum computers. *Nature* 464, 7285 (2010), 45.
- [45] Ben P Lanyon, Till J Weinhold, Nathan K Langford, Marco Barbieri, Daniel FV James, Alexei Gilchrist, and Andrew G White. 2007. Experimental demonstration of a compiled version of Shor's algorithm with quantum entanglement. *Physical Review Letters* 99, 25 (2007), 250505.
- [46] Andrei Lapets, Marcus P da Silva, Mike Thome, Aaron Adler, Jacob Beal, and Martin Rötteler. 2013. QuaFL: A typed DSL for quantum programming. In *Proceedings of the 1st annual workshop on Functional programming concepts in domain-specific languages*. ACM, 19–26.
- [47] Allen Leung, Nicolas Vasilache, Benoît Meister, Muthu Baskaran, David Wohlford, Cédric Bastoul, and Richard Lethin. 2010. A Mapping Path for multi-GPGPU Accelerated Computers from a Portable High Level Programming Abstraction. In *Proceedings of the 3rd Workshop on General-Purpose Computation on Graphics Processing Units (GPGPU-3)*. ACM, New York, NY, USA, 51–61. <https://doi.org/10.1145/1735688.1735698>
- [48] Gushu Li, Yufei Ding, and Yuan Xie. 2019. Tackling the Qubit Mapping Problem for NISQ-Era Quantum Devices. In *Proceedings of the Twenty-Fourth International Conference on Architectural Support for Programming Languages and Operating Systems (ASPLOS '19)*. ACM, New York, NY, USA, 1001–1014. <https://doi.org/10.1145/3297858.3304023>
- [49] Amy W. Lim, Gerald I. Cheong, and Monica S. Lam. 1999. An Affine Partitioning Algorithm to Maximize Parallelism and Minimize Communication. In *Proceedings of the 13th International Conference on Supercomputing (ICS '99)*. Association for Computing Machinery, New York, NY, USA, 228–237. <https://doi.org/10.1145/305138.305197>
- [50] T Loke and JB Wang. 2016. OptQC v1.3: An (updated) optimized parallel quantum compiler. *Computer Physics Communications* 207 (2016), 531–532.
- [51] Enrique Martin-Lopez, Anthony Laing, Thomas Lawson, Roberto Alvarez, Xiao-Qi Zhou, and Jeremy L O'brien. 2012. Experimental realization of Shor's quantum factoring algorithm using qubit recycling. *Nature Photonics* 6, 11 (2012), 773.
- [52] Jarrod R McClean, Ian D Kivlichan, Damian S Steiger, Yudong Cao, E Schuyler Fried, Craig Gidney, Thomas Häner, Vojtěch Havlíček, Zhang Jiang, Matthew Neeley, et al. 2017. OpenFermion: The Electronic Structure Package for Quantum Computers. *arXiv preprint arXiv:1710.07629* (2017).
- [53] Prakash Murali, Jonathan M. Baker, Ali Javadi-Abhari, Frederic T. Chong, and Margaret Martonosi. 2019. Noise-Adaptive Compiler Mappings for Noisy Intermediate-Scale Quantum Computers. In *Proceedings of the Twenty-Fourth International Conference*

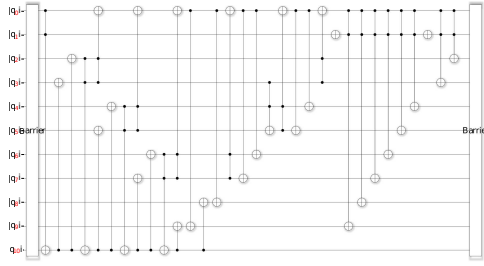
- on Architectural Support for Programming Languages and Operating Systems (ASPLOS '19). ACM, New York, NY, USA, 1015–1029. <https://doi.org/10.1145/3297858.3304075>
- [54] Dmitry Nadezhkin, Hristo Nikolov, and Todor Stefanov. 2013. Automated Generation of Polyhedral Process Networks from Affine Nested-Loop Programs with Dynamic Loop Bounds. *ACM Trans. Embed. Comput. Syst.* 13, 1s, Article 28 (Dec. 2013), 24 pages. <https://doi.org/10.1145/2536747.2536750>
- [55] Jennifer Paykin, Robert Rand, and Steve Zdancewic. 2017. QWIRE: A Core Language for Quantum Circuits. In *Proceedings of the 44th ACM SIGPLAN Symposium on Principles of Programming Languages (POPL 2017)*. ACM, New York, NY, USA, 846–858. <https://doi.org/10.1145/3009837.3009894>
- [56] Massimiliano Poletto and Vivek Sarkar. 1999. Linear Scan Register Allocation. *ACM Trans. Program. Lang. Syst.* 21, 5 (Sept. 1999), 895–913. <https://doi.org/10.1145/330249.330250>
- [57] Louis-Noël Pouchet, Peng Zhang, P. Sadayappan, and Jason Cong. 2013. Polyhedral-based Data Reuse Optimization for Configurable Computing. In *Proceedings of the ACM/SIGDA International Symposium on Field Programmable Gate Arrays (FPGA '13)*. ACM, New York, NY, USA, 29–38. <https://doi.org/10.1145/2435264.2435273>
- [58] IBM Research. 2017. IBM Q Experience. (2017). <https://www.research.ibm.com/ibm-q/>
- [59] Revlib. 2020. Revlib: An Online Resource for Reversible Functions and Circuits. (2020). <http://www.revlib.org/functions.php> Online; accessed on August 2020.
- [60] Peter W Shor. 1994. Algorithms for quantum computation: Discrete logarithms and factoring. In *Foundations of Computer Science, 1994 Proceedings., 35th Annual Symposium on*. Ieee, 124–134.
- [61] Peter W Shor. 1999. Polynomial-time algorithms for prime factorization and discrete logarithms on a quantum computer. *SIAM review* 41, 2 (1999), 303–332.
- [62] Marcos Yukio Siraichi, Vinicius Fernandes dos Santos, Sylvain Collange, and Fernando Magno Quintao Pereira. 2018. Qubit Allocation. In *Proceedings of the 2018 International Symposium on Code Generation and Optimization (CGO 2018)*. ACM, New York, NY, USA, 113–125. <https://doi.org/10.1145/3168822>
- [63] Robert S Smith, Michael J Curtis, and William J Zeng. 2016. A practical quantum instruction set architecture. *arXiv preprint arXiv:1608.03355* (2016).
- [64] Mathias Soeken, Stefan Frehse, Robert Wille, and Rolf Drechsler. 2011. RevKit: An open source toolkit for the design of reversible circuits. In *International Workshop on Reversible Computation*. Springer, 64–76.
- [65] Mathias Soeken, Stefan Frehse, Robert Wille, and Rolf Drechsler. 2012. RevKit: A Toolkit for Reversible Circuit Design. *Multiple-Valued Logic and Soft Computing* 18, 1 (2012), 55–65.
- [66] Mathias Soeken, Thomas Haener, and Martin Roetteler. 2018. Programming quantum computers using design automation. In *Design, Automation & Test in Europe Conference & Exhibition (DATE), 2018*. IEEE, 137–146.
- [67] Damian S Steiger, Thomas Häner, and Matthias Troyer. 2018. ProjectQ: an open source software framework for quantum computing. *Quantum* 2 (2018), 49.
- [68] Krysta Svore, Alan Geller, Matthias Troyer, John Azariah, Christopher Granade, Bettina Heim, Vadym Kliuchnikov, Mariia Mykhailova, Andres Paz, and Martin Roetteler. 2018. Q#: Enabling scalable quantum computing and development with a high-level DSL. In *Proceedings of the Real World Domain Specific Languages Workshop 2018*. ACM, 7.
- [69] Yasuhiro Takahashi and Noboru Kunihiro. 2008. A Fast Quantum Circuit for Addition with Few Qubits. *Quantum Info. Comput.* 8, 6 (July 2008), 636–649. <http://dl.acm.org/citation.cfm?id=2016976.2016981>
- [70] Nicolas Vasilache. 2007. *Scalable Program Optimization Techniques in the Polyhedra Model*. Ph.D. Dissertation. University of Paris-Sud 11.
- [71] Vlatko Vedral, Adriano Barenco, and Artur Ekert. 1996. Quantum networks for elementary arithmetic operations. *Physical Review A* 54, 1 (Jul 1996), 147–153. <https://doi.org/10.1103/physrevA.54.147>
- [72] Anand Venkat, Mary Hall, and Michelle Strout. 2015. Loop and Data Transformations for Sparse Matrix Code. In *Proceedings of the 36th ACM SIGPLAN Conference on Programming Language Design and Implementation (PLDI '15)*. ACM, New York, NY, USA, 521–532. <https://doi.org/10.1145/2737924.2738003>
- [73] Anand Venkat, Manu Shantharam, Mary Hall, and Michelle Mills Strout. 2014. Non-affine Extensions to Polyhedral Code Generation. In *Proceedings of Annual IEEE/ACM International Symposium on Code Generation and Optimization (CGO '14)*. ACM, New York, NY, USA, Article 185, 10 pages. <https://doi.org/10.1145/2581122.2544141>
- [74] Sven Verdoolaege. 2009. Polyhedral process networks. (2009). [https://lirias.kuleuven.be/retrieve/91003/\\$D\\$Presentation\[freelyavailable\]](https://lirias.kuleuven.be/retrieve/91003/DPresentation[freelyavailable])
- [75] Sven Verdoolaege. 2010. isl: An Integer Set Library for the Polyhedral Model. In *ICMS*, Vol. 6327. Springer, 299–302.
- [76] Sven Verdoolaege. 2011. Counting affine calculator and applications. In *First International Workshop on Polyhedral Compilation Techniques (IMPACT'11)*, Chamonix, France.
- [77] Sven Verdoolaege, Juan Carlos Juega, Albert Cohen, José Ignacio Gómez, Christian Tenllado, and Francky Catthoor. 2013. Polyhedral Parallel Code Generation for CUDA. *ACM Trans. Archit. Code Optim.* 9, 4, Article 54 (Jan. 2013), 23 pages. <https://doi.org/10.1145/2400682.2400713>
- [78] Dave Wecker and Krysta M Svore. 2014. LIQUI>: A software design architecture and domain-specific language for quantum computing. *arXiv preprint arXiv:1402.4467* (2014).
- [79] R. Wille, D. Große, L. Teuber, G. W. Dueck, and R. Drechsler. 2008. RevLib: An Online Resource for Reversible Functions and Reversible Circuits. In *Int'l Symp. on Multi-Valued Logic*. 220–225. RevLib is available at <http://www.revlib.org>.
- [80] Ze-Liang Xiang, Sahel Ashhab, JQ You, and Franco Nori. 2013. Hybrid quantum circuits: Superconducting circuits interacting with other quantum systems. *Reviews of Modern Physics* 85, 2 (2013), 623.
- [81] A. Zulehner, A. Paller, and R. Wille. 2018. Efficient mapping of quantum circuits to the IBM QX architectures. In *2018 Design, Automation Test in Europe Conference Exhibition (DATE)*. 1135–1138. <https://doi.org/10.23919/DATE.2018.8342181>

Appendix A

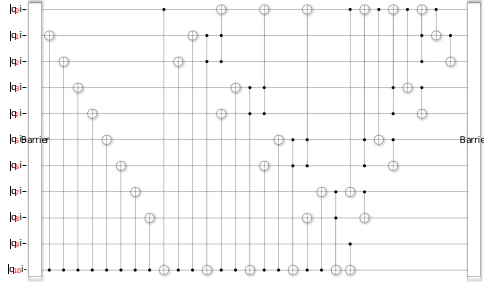
Due to space constraints and for better viewing, we include the set of evaluated circuits in this appendix. The set of circuit benchmarks evaluated in our work are summarized in Tab.3. These should be viewed as small computational building blocks used in larger applications, in similar spirit to modern and classic computational kernels such as DGEMM.

Here we quickly summarize their overall role/goal:

- `sum5,init-G5`: Sub-circuits used in [69] corresponding to the computation of initial values and sum of an adder. The circuits do not use ancillary qubits, and have depth $O(n)$. The corresponding circuit diagrams shown in Fig.10.
- `pipelined-swap`: Performs a qubit SWAP operation between two qubits $2N$ lanes apart. We show in Fig.9 its implementation in **AXL**, and its circuit diagram in Fig.11.
- `cnt3-5_179`: A 5 digit binary coded ternary counter with count control input (cnt) [79]. Circuit diagram shown in Fig.12.



(a) init-G₅ [69]



(b) sum5 [69]

Figure 10. init-G₅ and sum5 circuits

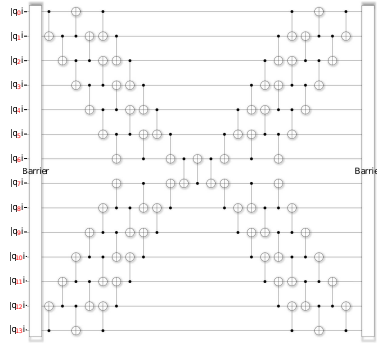
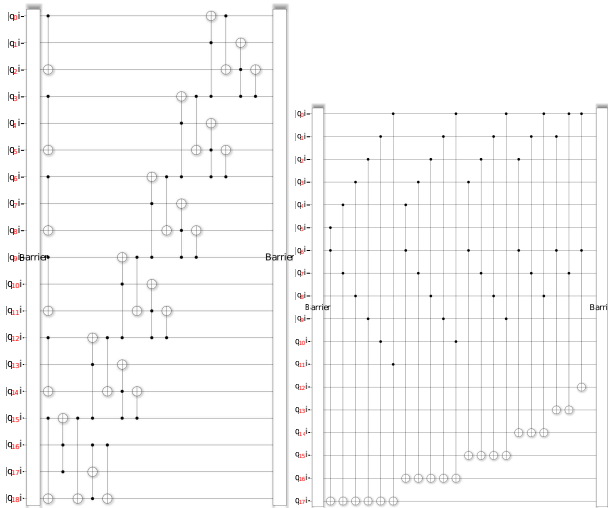


Figure 11. pipelined-swap [27]



(a) cnt3-5_179 [79]

(b) cheung [17]

Figure 12. cnt3-5_179 and cheung circuits

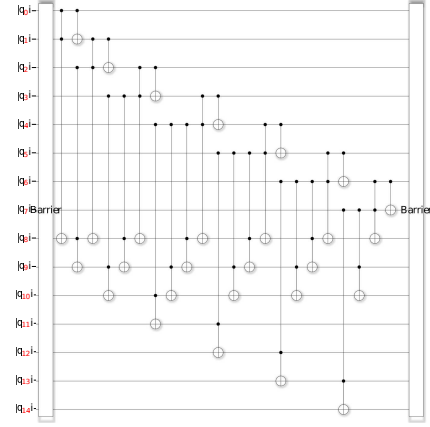


Figure 13. rd84_142 [79]

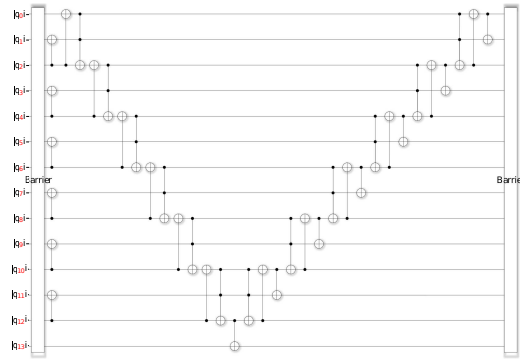
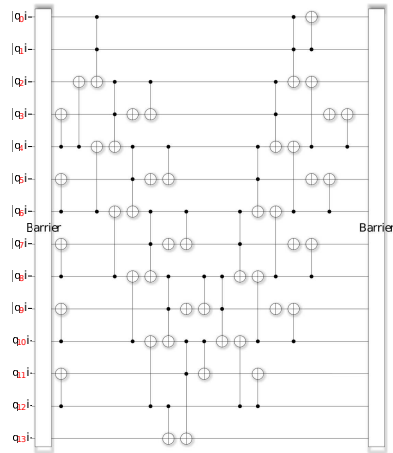
```

1  param N;
2  statement S1a, S1b, S1c;
3  statement S2a, S2b, S2c;
4  statement S3;
5  statement S4a, S4b, S4c;
6  statement S5a, S5b, S5c;
7
8  S1a := {i: 0<=i<N (%) #CNOT(i, i+1) };
9  S1b := {i: 0<=i<N (%) #CNOT(i+1, i) };
10 S1c := {i: 0<=i<N (%) #CNOT(i, i+1) };
11
12 S2a := {i: 0<=i<N (%) #CNOT(2*N-i+1, 2*N-i) };
13 S2b := {i: 0<=i<N (%) #CNOT(2*N-i, 2*N-i+1) };
14 S2c := {i: 0<=i<N (%) #CNOT(2*N-i+1, 2*N-i) };
15
16 S3 := {i: i = N (%) #CNOT(i, i+1) (+)
17       #CNOT(i+1, i) (+) #CNOT(i, i+1) };
18
19 S4a := {i: 0<=i<N (%) #CNOT(N-i-1, N-i) };
20 S4b := {i: 0<=i<N (%) #CNOT(N-i, N-i-1) };
21 S4c := {i: 0<=i<N (%) #CNOT(N-i-1, N-i) };
22
23 S5a := {i: 0<i<=N (%) #CNOT(N+i+1, N+i) };
24 S5b := {i: 0<i<=N (%) #CNOT(N+i, N+i+1) };
25 S5c := {i: 0<i<=N (%) #CNOT(N+i+1, N+i) };
26
27 codegen { S1a (+) S1b (+) S1c (+) S2a (+)
28           S2b (+) S2c (+) S3 (+) S4a (+) S4b (+)
29           S4c (+) S5a (+) S5b (+) S5c } with { N=6};

```

Figure 9. AXL implementation of pipelined-swap circuit

- cheung: sub-circuit used in computing the \vec{d} component of the Elliptic Curve Discrete Logarithm problem (ECDLP) [17]. Circuit diagram shown in Fig.12.

(a) adder-maj-uma [22], $N=6$ 

(b) cuccaro-adder-6bit [22]

- `rd84_142`: Counts the number of ones in the input [79]. Circuit diagram shown in Fig.13.
- `adder-maj-uma`: is a ripple-carry adder using the in-place “MAJority” (MAJ) and “UnMajority and Add” (UMA) patterns [22]. Circuit diagram shown in Fig.14.
- `cuccaro-adder-6bit`: Depth optimized ripple-carry adder of depth $2n + 4$, with $2n - 1$ time slices and 5 CNOT time-slices [22]. Circuit diagram shown in Fig.14.

Figure 14. adder-maj-uma and cuccaro-adder-6bit circuits